Fuel 262 (2020) 116488

Contents lists available at ScienceDirect

Fuel

journal homepage: www.elsevier.com/locate/fuel

Full Length Article

Understanding the thermal behaviour of blends of biodiesel and diesel: Phase behaviour of binary mixtures of alkanes and FAMEs

Nuno F.M. Branco[a,b,c], Ana I.M.C. Lobo Ferreira[a], Jorge C. Ribeiro[b], Luís M.N.B.F. Santos[a,*], João A.P. Coutinho[c,*]

[a] CIQUP, Departamento de Química e Bioquímica, Faculdade de Ciências da Universidade do Porto, P4169-007 Porto, Portugal
[b] CICECO, Departamento de Química, Universidade de Aveiro, P3819-193 Aveiro, Portugal
[c] GALP, Refinaria de Leça, Matosinhos, Portugal

GRAPHICAL ABSTRACT

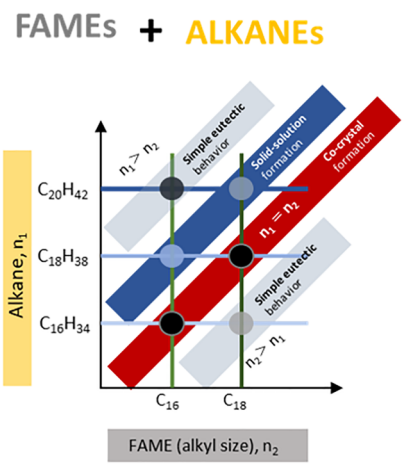

ARTICLE INFO

Keywords:
Alkanes
FAME
Phase behaviour: DSC
Co-crystallization
Solid solutions
Eutectic
Binary mixture

ABSTRACT

The study of the phase behaviour of binary mixtures of fatty acid methyl esters (FAME) and alkanes are here studied to understand the behaviour of the mineral diesel/biodiesel blends. Six binary mixtures of the most common saturated methyl esters (methyl stearate or methyl palmitate) with a saturated alkane (hexadecane, octadecane or eicosane) were evaluated by differential scanning calorimetry (DSC), X-ray diffraction (XRD) and optical microscopy. The binary mixtures studied show a more complex phase behaviour than previously reported, which it is shown to be dependent of the size difference between the alkyl chain length of the esters and the alkanes. It was found that in mixtures with equal alkyl chain length a co-crystal is formed, and when the alkane chain length is larger than in the FAME by two methylene groups the formation of a solid-solution increasing significantly the solid phase stability is observed. The results and conclusions derived from the phase behaviour of this set of binary mixtures, between alkanes and methyl esters, can be used as a model for the interpretation of the cloud and pour points increase in biodiesel blends (in special the ones with a rich fraction of methyl palmitate or methyl stearate when combined with mineral diesel with high content of octadecane or eicosane respectively).

* Corresponding authors.
E-mail addresses: lbsantos@fc.up.pt (L.M.N.B.F. Santos), jcoutinho@ua.pt (J.A.P. Coutinho).

https://doi.org/10.1016/j.fuel.2019.116488
Received 8 January 2019; Received in revised form 17 October 2019; Accepted 22 October 2019

1. Introduction

Fossil fuels have well know adverse environmental effects such as the emission of CO_2 and SO_2, and their production is limited to a few regions often fraught with political problems. For those reasons a considerable effort has been developed to replace them for more sustainable and renewable sources of energy [1].

Biofuels are environmentally friendly fuels that can be produced from renewable feedstocks reducing the dependency on oil imports, and CO_2 emissions [2]. One of the most used biofuels is biodiesel that is "a fuel comprised of monoalkyl esters of long-chain fatty acids made from natural, renewable sources such as new/used vegetable oils or animal fats" [3]. Biodiesel has a lot of advantages since it is renewable, energy efficient, biodegradable, and has a high cetane number. Besides, one of its main advantages is its similarity with conventional diesel that allows it to be used in conventional diesel engines, without any engine modification, or to be blended with diesel in any proportion, improving its lubricity, and ignition quality. Biodiesel has a lead role on the alternatives to petrol fuel, but some challenges must be overcome to optimize their production, usability, sustainability and to decrease their environmental impact [2,4,5].

One of the problems with biodiesel is its behaviour at low temperatures, since it has higher cloud and pour points than mineral diesel [6,7], what could lead to the formation of solid deposits that clog fuel filters in vehicles or cause blockage in the fuel lines, leading to fuel starvation in engine operation [8–13]. The low temperature properties of biodiesel are controlled by several specifications, such as pour point (PP) (ASTM D-97, ASTM D-5949), cold filter plugging point (CFPP) ((EN 116, IP-309, ASTM D-6371), cloud point (CP) (EN 23015, ASTM D-2500), and the low-temperature filterability test, LTFT (ASTM D-4539). This is particularly important in cold regions during winter months [14–17].

The biodiesel is mainly produced by transesterification of oils and fats with an alcohol and so the final composition depends on the source of the oil and the alcohol used in the esterification. The biodiesel composition is an important factor in the definition of its cold flow properties. The biodiesel fuels with significant amounts of saturated fatty compounds show a higher CP and PP due to the high melting point of the saturated fatty compounds [18]. There are studies showing that the cloud point of biodiesel could be determined by the amount of saturated fatty acid methyl esters (FAME) regardless the composition of unsaturated esters [19].

The solid–liquid equilibrium of fatty acid methyl and ethyl esters has been extensively studied [6,20–22], nevertheless the phase behaviour of binary mixtures of fatty acid esters and hydrocarbons has been poorly investigated. There are only a few studies of ethyl esters or methyl esters with aromatic hydrocarbons [23] and linear alkanes [24–27]. Typically, the phase diagrams of these mixtures exhibits invariant points, such as eutectics and peritectics. The interpretation of their phase diagrams is fundamental for the understanding the low temperature phase behaviour of blends of biodiesel and diesel fuels [20,23–26].

The binary mixtures of FAMEs composed by methyl myristate, methyl palmitate and methyl stearate were studied by Costa et al. [22] that showed that these mixtures present very complex phase behaviour with multiple phase regions and peritectic and metatectic reactions.

Maximo et al. [20] studied the blends of FAME with FAEE with mixtures as ethyl palmitate, ethyl stearate or ethyl oleate with methyl palmitate. These systems showed also a very complex behaviour with the formation of solid-solutions, peritectic reactions and metatectic transitions. The authors proposed that the mixtures of FAME with FAEE could be used to improve their cold flow properties when compared with mixtures of FAMEs.

The systems of FAMEs with aromatics were studied by Benziane et al. [23] that concluded that all the mixtures studied presented a simple eutectic behaviour. In another work Benziane et al. [24] studied the FAMEs (methyl palmitate and methyl stearate) in mixtures with heavy alkanes (*n*-eicosane, *n*-tetracosane and *n*-octacosane) again reporting that these mixtures had a simple eutectic behaviour. A similar conclusion was reported by Lobbia et al. with the study of the crystallization curve of the methyl stearate, methyl nonadecanoate, ethyl stearate and methyl palmitate with hexadecane [27].

Mixtures between FAEE and alkanes were studied by Robustillo et al. [25] reporting systems of ethyl laurate, ethyl palmitate and *n*-decane and by Chabane et al. [26] which studied mixtures of ethyl myristate with n-tetradecane and n-hexadecane and ethyl palmitate with n-octadecane. All the systems were reported to present a simple eutectic behaviour except for the system ethyl laurate and *n*-decane were a peritectic point was also identified. Some of these systems show the presence of solid–solid transitions.

Since pure biodiesel is seldom used, most of it being sold as blends with mineral diesel, it would be very important to study the phase behaviour of the mixtures of the most abundant saturated fatty acid methyl esters in biodiesel with n-alkanes. The mixtures of dissimilar

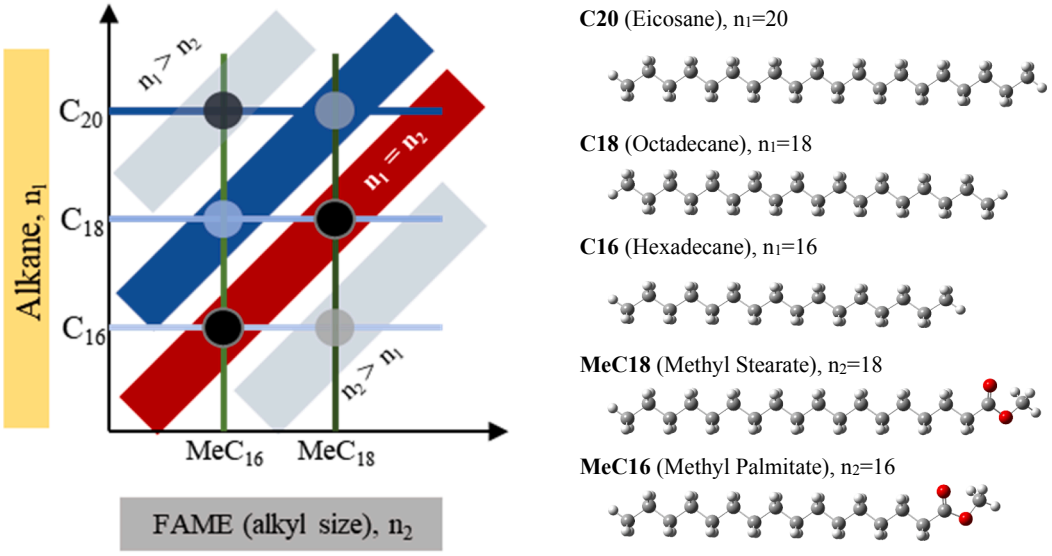

Fig. 1. Schematic representation of the binary mixtures between methyl esters and alkanes studied in this work. Alkanes: Eicosane, $C_{20}H_{42}$, (C20); Octadecane, $C_{18}H_{38}$, (C18); Hexadecane, $C_{16}H_{34}$, (C16); FAMEs: Methyl stearate, $C_{19}H_{38}O_2$, (MeC18); Methyl palmitate, $C_{17}H_{34}O_2$, (MeC16).

size are well established to produce simple eutectic systems with a near ideal behaviour [24–26].

This work presents a systematic study of the phase behaviour of binary mixtures composed by combination of the most abundant saturated FAMEs with the n-alkanes with similar size as depicted schematically in Fig. 1. The phase diagrams of these two FAMEs, methyl palmitate (MeC16) and methyl stearate (MeC18) with hexadecane (C16), octadecane (C18) and eicosane (C20) were studied in detail using differential scanning calorimetry (DSC), temperature controlled polarized optical microscopy, and x-ray powder diffraction, XRD. The DSC is rapid and a sensitive technique that is able to determine accurately the temperature and the heat involved in the phase transition [28–30]. The results and its relevance to the behaviour of blends of diesel with biodiesel will be discussed below.

2. Experimental

2.1. Materials

All the compounds used in this study were supplied by Sigma-Aldrich. The stated purity presented by the supplier and the purity of the samples evaluated in our laboratory using gas chromatography (HP 4890 equipped with a cross-linked, 5% diphenyl and 95% dimethylpolysiloxane column), is depicted in Table 1. The relative atomic masses used were those recommended by IUPAC in 2013 [31]. Due to their high quality the samples were handled without any further purification.

Binary mixtures of around 200 mg with different compositions (molar fraction between 0.0 and 1.0 in 0.1 mol fraction steps) were prepared gravimetrically (using an analytical balance, Mettler Toledo, model AG245, with a mass resolution of ± 0.01 mg) and kept in sealed glass bottles to avoid contamination. The mixtures were heated to a higher temperature than the melting point of the pure components (315 K) mixed and kept overnight in order to obtain a homogeneous solution. Some additional binary mixtures were prepared, using the same procedure, whenever necessary to increase the definition/resolution of the phase diagrams. The overall uncertainty of the experimental mole fraction was estimated to be approximately $\pm\ 1 \times 10^{-3}$.

2.2. Differential scanning calorimetry

The thermal study of each sample was evaluated by DSC, using two different commercial DSC instruments (Perkin-Elmer model Pyris Diamond DSC and NETZSCH 200F3 DSC) using in both instruments high purity (99.999%) gaseous nitrogen as protective gas (50 ml·min^{-1}). The temperature and heat flux scales of the power compensation DSC (Perkin-Elmer model Pyris Diamond) were calibrated by measuring the temperature and the enthalpy of fusion of reference materials [32–34] namely, benzoic acid, 4-methoxybenzoic acid, triphenylene, naphthalene, anthracene, 1,3,5-triphenylbenzene, phenylacetic acid, perylene, *ortho*-terphenyl, and 9,10-diphenylanthracene, indium and water at different scanning rates (2, 5, and 10 K·min^{-1}). The temperature and heat flux scales of the DSC (Netzsch model 200F3) were calibrated based in the temperature and the enthalpy of fusion of the following reference materials: benzoic acid, *o*-terphenyl, cyclohexane, adamantane, undecane and water [32–34].

For the thermal study, small quantities of each sample were sealed in an aluminium crucible (30/50 μg) and heated at a rate of 5 K·min^{-1} to 323.15 K under nitrogen atmosphere. The sample was maintained at this temperature for 5 min and was then cooled at a rate of 5 K·min^{-1} to a temperature of 223.15 K and maintained at this temperature for 10 min. After this isothermal step, the sample was then heated at a scanning rate of 2 K·min^{-1} until the complete melting and an isothermal step of 5 min. Due to peaks overlapping, which prevents the direct evaluation of the onset temperature, the solid–solid and solid–liquid transitions were evaluated based on the peak temperatures [6,20,22,35] and corrected to the temperature delay estimated by the difference between the onset and the peak temperatures observed in the runs with the pure compounds (DSC with identical experimental conditions: sample mass, temperature scanning rate). For the DSC (Perkin-Elmer model Pyris Diamond) temperature correction “Peak” to “Onset” were typically in the order of – 1.2 K (Onset_T = Peak_T – 1.2), for the DSC (Netzsch model 200F3) the same corrections were slightly higher in the order of – 2.0 K (Onset_T = Peak_T – 2.0), for the scanning rate of 2 K·min^{-1}. Additional details could be found as Supporting information.

The uncertainty of the experimental results was taken as the overall standard deviation for the enthalpies of melting, σ, and was estimated as ± 0.5 K for the temperature and 2% for the heat involved in the melting process (typical ± 4 J·g^{-1} considering the size and the average molar mass of the samples).

2.3. Phase transition morphology analyses

The morphology analysis of the solid phases of the mixtures, and the solid–solid and solid–liquid phase transitions observed by DSC were explored by optical microscopy using an Olympus optical system, model BX51, equipped with a Linkam T95-PE temperature controller with LTS120, and a camera Olympus DP71 with U-CMAD3/U-TV1x-2.

The qualitative characterization of the crystal structures of the solid phases was carried by x-ray powder diffraction in a Panalytical XRD apparatus model Empyrean, operating with an anode of Cu ($K_{\alpha1}$ = 1.5406 Å; $K_{\alpha2}$ = 1.5444 Å). The low temperature chamber was an Anton Paar model TTK450, the temperature controller an Anton Paar TCU100 and the chamber was cooled using liquid nitrogen. Diffraction data were collected in the 2θ range from 3° to 50° in steps of 0.02 and a time per step of 50 s using a linear detector PIXEL 1D with an active length 3.347°, with incident slit of ¼° and diffracted beams anti-scatter slits of 7.5 mm. The diffractograms acquired for these mixtures did not have enough resolution to allow the crystal structures to be derived from them. They were only used to identify differences between the solid regions comparing the diffractograms at different temperatures and concentrations. The samples were heated or cooled until the desired temperature at which the diffraction data were collected. The heating or cooling process of the sample was conduct by the temperature controller with no programmed temperature rate [36,37].

3. Results

Given the limited information available about the phase behaviour of systems composed of fatty acid methyl esters and alkanes, the main components of waxes forming in biodiesel and mineral diesel, the phase

Table 1
Compounds description, experimental and suppliers purities (%(m/m)).

Chemicals name	Chemical formula	Molecular weight/g·mol^{-1}	CASno.	Purity/GC	Purity/supplier
Hexadecane	$C_{16}H_{34}$	226.42	544–76-3	99.6	> 99
Octadecane	$C_{18}H_{38}$	254.47	593–45-3	99.1	99
Eicosane	$C_{20}H_{42}$	282.52	112–95-8	99.6	99
Methyl Palmitate	$C_{17}H_{34}O_2$	270.43	112–39-0	99.8	> 99
Methyl Stearate	$C_{19}H_{38}O_2$	298.48	112–61-8	99.7	99

diagrams of several of these mixtures are here measured and analysed.

The phase diagrams reported below are the result of the interpretation of the DSC thermograms, from which, whenever possible Tammann plots are presented to help identification and interpretation of eutectic points and the solid solution domains. These results were complemented with information derived from optical microscopy where it is possible to observe some visual changes in solid structure or the initial/final melting temperatures. The results are further supported by XRD where is possible to observe the crystal structures changes with temperature and concentration. The melting properties of the pure compounds are reported in Table 2.

The phase behaviour results were compared with the prediction of an ideal eutectic behaviour described by the Solid-Liquid equilibrium equation that describes the dependence of the liquidus line temperature with the mole fraction, $T(x_i)$, the liquid mixture being assumed as an ideal liquid solution, and neglecting the correction effect of the difference in the heat capacities between the solid and liquid phases.

$$\ln(x_i) = \frac{\Delta H_{fus}}{R}\left(\frac{1}{T_{fus_i}} - \frac{1}{T(x_i)}\right) \quad (1)$$

In this equation x_i is mole fraction of the component i, $T_{fus\ i}$ and ΔH_{fus} are the melting and heat of fusion of the pure component, and R is the universal gas constant. This equation was only used for comparative proposes between the different binary systems and should not be considered an attempt to describe the observed thermal behaviour.

3.1. Phase behaviour of the binary mixture methyl stearate + hexadecane (MeC18 + C16)

Fig. 2 shows the solid–liquid phase diagram measured at atmospheric pressure (p = 0.10 ± 0.01 MPa) for the system composed by methyl stearate and hexadecane (MeC18 + C16). The thermograms are depicted in Fig. SI.1. It was found that the (MeC18 + C16) system presents a simple eutectic type behaviour with an eutectic composition close to x_A = 0.15 and an eutectic temperature of 289 K in good agreement with the results published by Lobbia et al. [27]. An invariant solid–solid transition at 278 K was found in this binary mixture in the intermediate binary mixtures compositions.

The solid–solid transition identified by DSC is not observable by optical microscopy. It shows a small endothermic and reversible heat of transition which was correlated with the hexadecane content as shown in the Tammann plot presented in Fig. 3. This suggests that the solid phase that undergoes the solid–solid transition is formed by hexadecane crystallizing on a solution of MeC18 on a structure not present when hexadecane is crystallized from the melt.

The structural change involved in this solid–solid transition was explored by XRD. The change in the XRD spectra with the temperature is depicted in Fig. 4 for the mixture with a composition of x = 0.25 of methyl stearate. The XRD data of the mixtures was compared with the XRD of the pure compounds. In the spectra regions highlighted by the regions "a" and "c" two new diffractions peaks at $2\theta = 23°$ and $2\theta = 26°$, are depicted, as well as a decrease of the peak intensity at $2\theta = 24°$, region "b", supporting the existence of a structural change in the crystal which is not observed in the pure hexadecane.

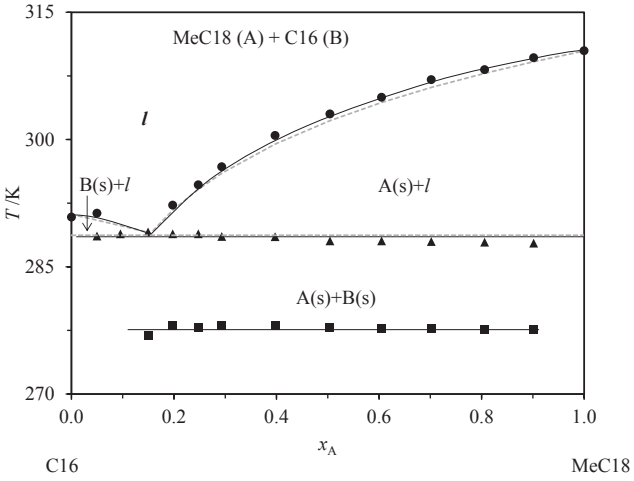

Fig. 2. Solid-liquid phase diagram (p = 0.10 ± 0.01 MPa) for the binary system methyl stearate (A) and hexadecane (B): ● – liquidus line; ■ – solid–solid transition; ▲ – eutectic transition. Dashed grey lines (—) indicates the ideal liquidus line.

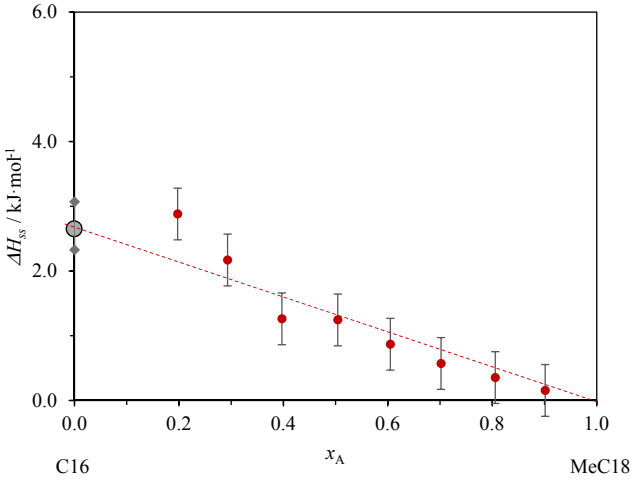

Fig. 3. Tammann diagram for the solid–solid transition for the binary system methyl stearate (A) + hexadecane (B). Solid-solid transition observed at T = 278 ± 1 K. Linear dependence with hexadecane mole fraction, converging to X_A = 1.0, ΔH_{ss} = 2.5 ± 0.5 kJ·mol^{-1} (hexadecane).

Table 2
Melting properties of the pure compounds studied.

Component name	T_{fus}/K this work	T_{fus}/K literature	ΔH_{fus}/J·g^{-1} this work	ΔH_{fus}/J·g^{-1} literature
Hexadecane	290.9 ± 0.5	291.1[a]	235 ± 4	228.79 ± 0.4[a]
Octadecane	300.3 ± 0.5	301.3[a]	235 ± 4	241.29 ± 0.4[a]
Eicosane	309.2 ± 0.5	309.7[a]	260 ± 5	238.21 ± 0.4[a]
Methyl palmitate	301.7 ± 0.5	300.53 ± 0.02[b]	202 ± 4	209.0 ± 4.6[b]
		305.15[c]		207.05 ± 7.8[c]
		302.2[d]		215[d]
Methyl Stearate	310.5 ± 0.5	310.16 ± 0.05[b]	218 ± 4	222.0 ± 1.8[b]
		310.9[c]		206.7 ± 5.7[c]
		311.0[d]		240[d]

"a" – reference [38]; "b" – reference [39]; "c" – reference [40]; "d" – reference [41]; Temperature and specific enthalpy uncertainty: taken as the overall standard deviation, σ, including the calibration uncertainty. Estimated as σ (temperature) = ± 0.5 K and σ (specific enthalpy of fusion) = ± 4 J·g^{-1}).

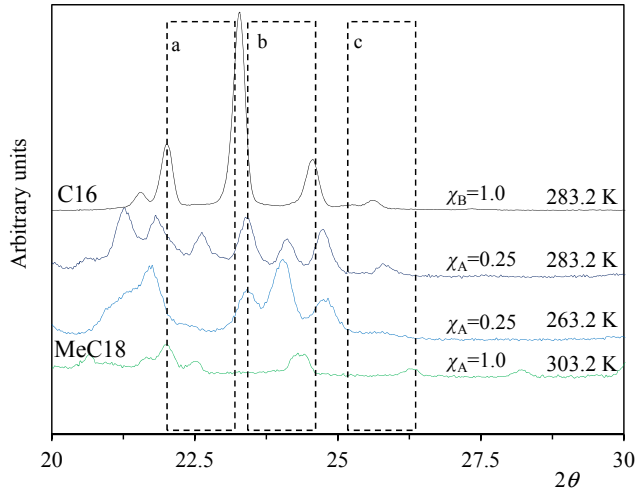

Fig. 4. XRD spectra for the solid–solid transition observed in binary mixtures composed by methyl stearate (A) and hexadecane (B).

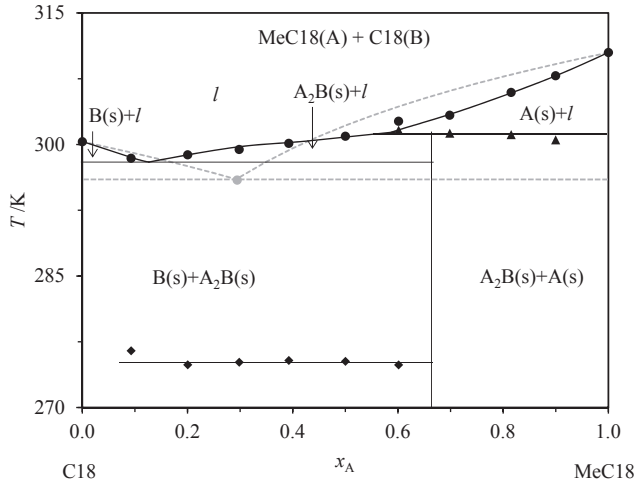

Fig. 5. Solid-liquid phase diagram (p = 0.10 ± 0.01 MPa) for the binary system methyl stearate (A) and octadecane (B): ● – liquidus line; ♦ – solid–solid transition; ▲ – peritectic transition. Dashed grey lines (—) indicates the ideal liquidus line.

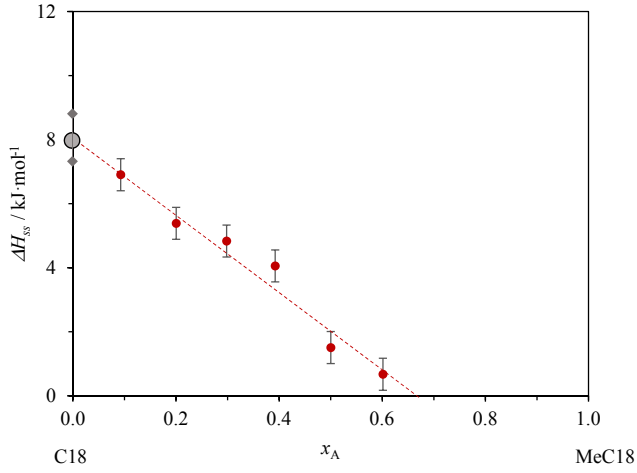

Fig. 6. Tammann diagram for the solid–solid transition for the binary system methyl stearate (A) and octadecane (B). Solid-solid transition observed at T = 275 ± 1 K. Linear dependence with octadecane mole fraction, converging to X_A = 0.66, ΔH_{ss} = 8.0 ± 0.5 kJ·mol^{-1} (octadecane).

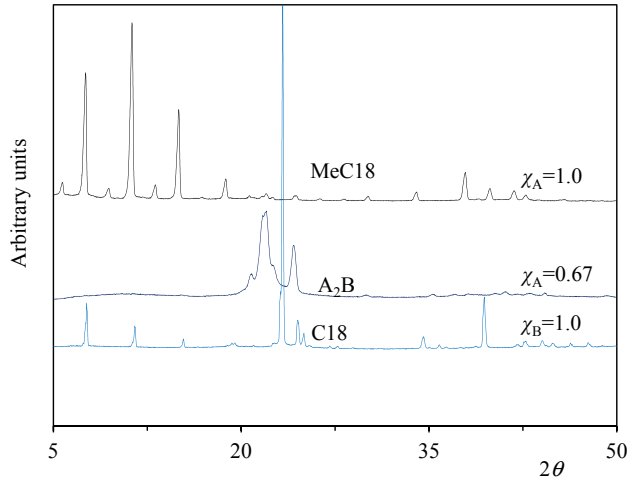

Fig. 7. XRD spectra for the pure compounds methyl stearate (A) and octadecane (B) at 298.2 K and the A_2B co-crystal formed at the 2:1composition.

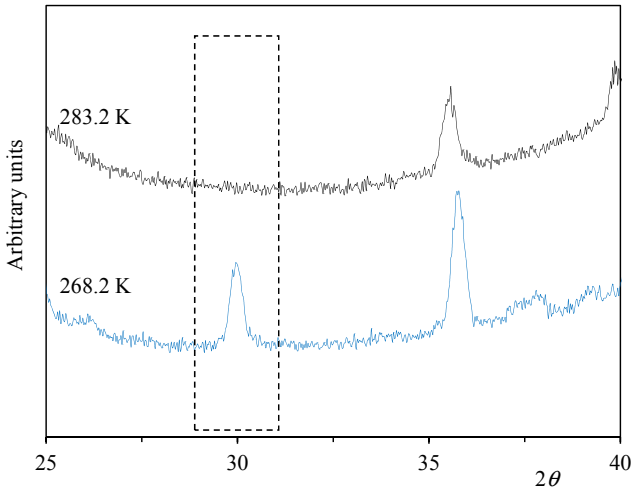

Fig. 8. XRD spectra for the binary system composed by 40% (mol/mol) methyl stearate and octadecane.

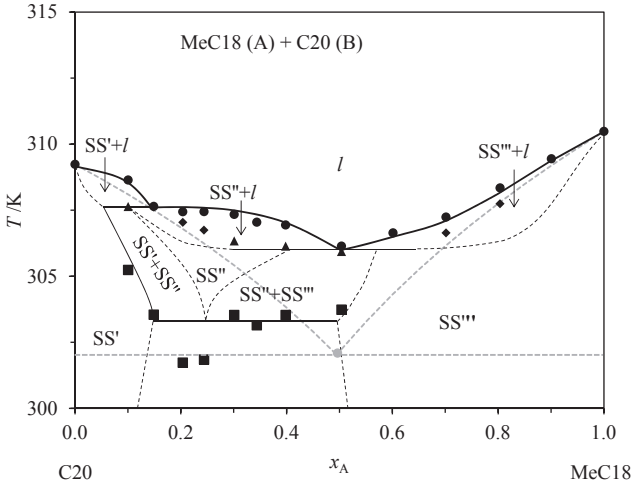

Fig. 9. Solid-liquid phase diagram (p = 0.10 ± 0.01 MPa) for the binary system methyl stearate (A) and eicosane (B): ● – liquidus line; ■ – solid–solid transition; ▲ – solidus line ♦ – possible metatectic transition. Dashed lines represent hypothetical transitions for which no evidence from DSC was available. Dashed grey lines (—) indicates the ideal liquidus line.

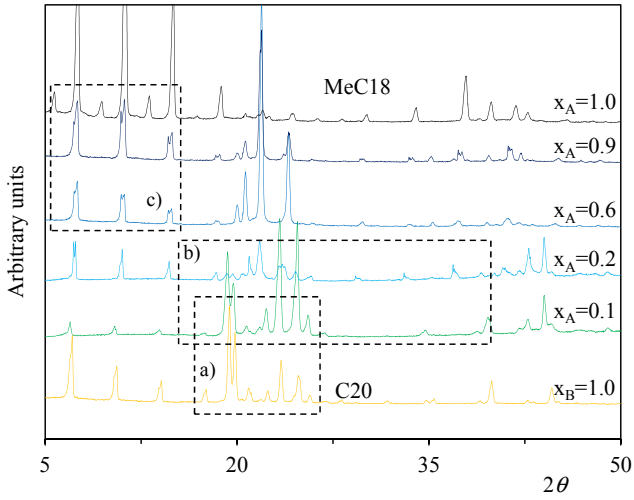

Fig. 10. XRD spectra for the binary system formed composed by methyl stearate (A) and eicosane (B) at 300 K.

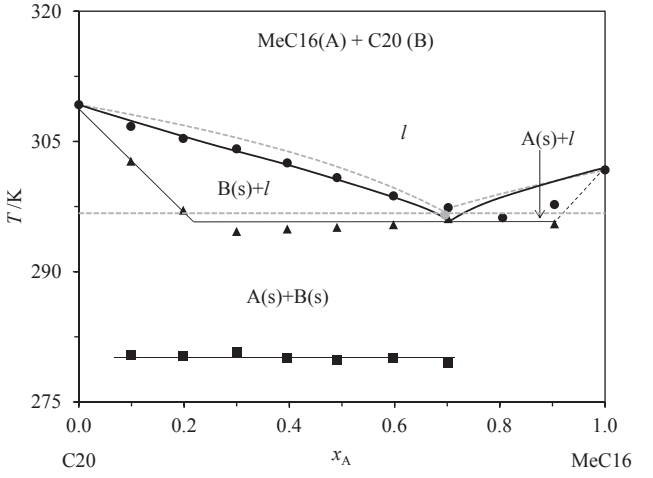

Fig. 11. Solid-liquid phase diagram (p = 0.10 ± 0.01 MPa) for the binary system methyl palmitate (A) + eicosane (B): ● – liquidus line temperature; ■ – solid–solid transition; ▲ – solidus line. Dashed grey lines (—) indicates the ideal liquidus line.

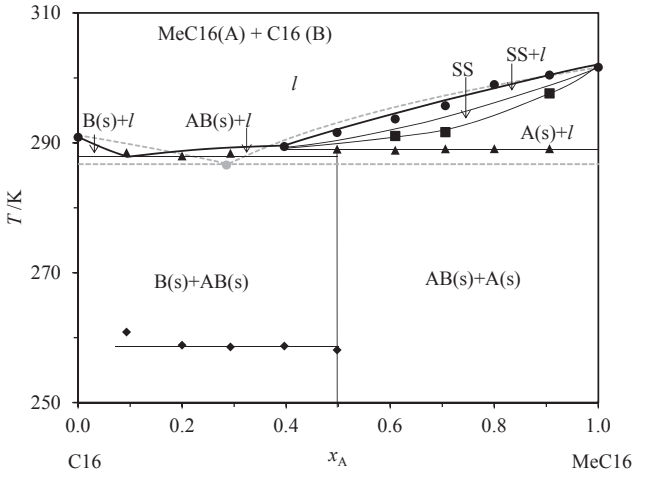

Fig. 12. Solid-liquid phase diagram (p = 0.10 ± 0.01 MPa) for the binary system formed by methyl palmitate (A) and hexadecane (B): ● – liquidus line; ■ – metatectic transition; ▲ – solidus line; ◆ – solid–solid transition. Dashed grey lines (—) indicates the ideal liquidus line.

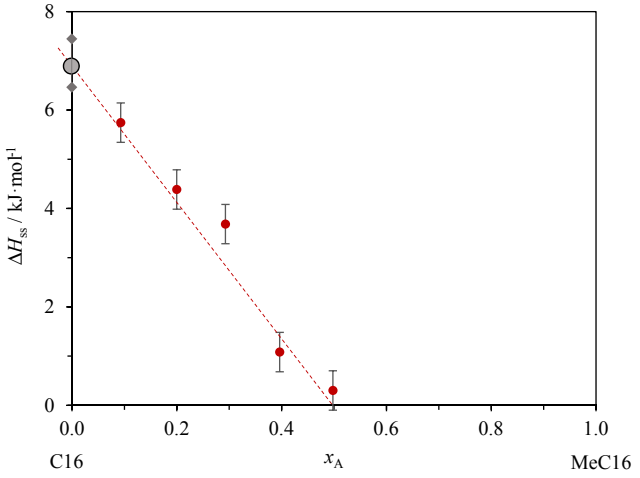

Fig. 13. Tammann diagram for the solid–solid transition for the binary system methyl palmitate (A) and hexadecane (B). Solid-solid transition observed at T = 258 ± 1 K. Linear dependence of hexadecane mole fraction, ΔH_{ss} = 7.0 ± 0.5 kJ·mol^{-1} (hexadecane).

3.2. Phase behaviour of the binary mixture methyl stearate + octadecane (MeC18 + C18)

The solid–liquid phase diagram for the binary mixture of methyl stearate + octadecane (MeC18 + C18) is presented in Fig. 5 and its thermograms in Fig. SI.2. This binary mixture presents novel features when compared with the previous phase diagram (MeC18 + C16). Here evidence to the formation of an intermediate compound, with a composition of x_A = 0.66, which suggests the 2:1 stoichiometric of FAME to alkane is found. The eutectic point was identified at T = 298 K and a molar fraction $x_A \sim 0.2$. The intermediate compound (2:1), decomposes at T = 300 K with the formation of a peritectic point at a composition close to x_A = 0.5. The composition ratio of the intermediate compound (2:1) was further supported by the Tammann plot of the solid–solid transition observed at 275 ± 1 K which converges to x_A = 0.66 as depicted in Fig. 6. Fig. 7 presents the XRD spectra of the two pure compounds and the intermediate compound (2:1). The comparative analysis the XRD spectra supports the formation of the intermediate compound identified from the phase diagram obtained from DSC.

Moreover, as mentioned above, this system also shows a solid–solid transition at about 275 K which is observable by DSC and XRD. The change in the crystal structure are supported by the XRD data as reported in Fig. 8 (2θ = 30° peak disappearance) highlighted in the dashed line box. The Tammann plot presented in Fig. 6 provides a strong indication that this solid–solid transition is associated to the octadecane, and is the octadecane analogous to the transition observed in the previous phase diagram for hexadecane. It is also quite interesting to observe that the octadecane solid–solid seems to be induced by its crystallization from the solution as it was not observed in pure octadecane.

3.3. Phase behaviour of the binary mixture methyl stearate + eicosane (MeC18 + C20)

The phase diagram for the binary system methyl stearate + eicosane (MeC18 + C20) is significantly more complex than the phase diagrams discussed previously. A significant number of phase transitions were observed by DSC at lower temperatures which indicates a much more complex behaviour. Fig. 9 presents our interpretation of the solid–liquid phase diagram for this binary mixture based in rationalization of the DSC thermograms depicted in Fig. SI.3. Here the solid lines correspond to actual observations of phase transitions while the black dashed lines are the suggestions of the missing phase transitions that

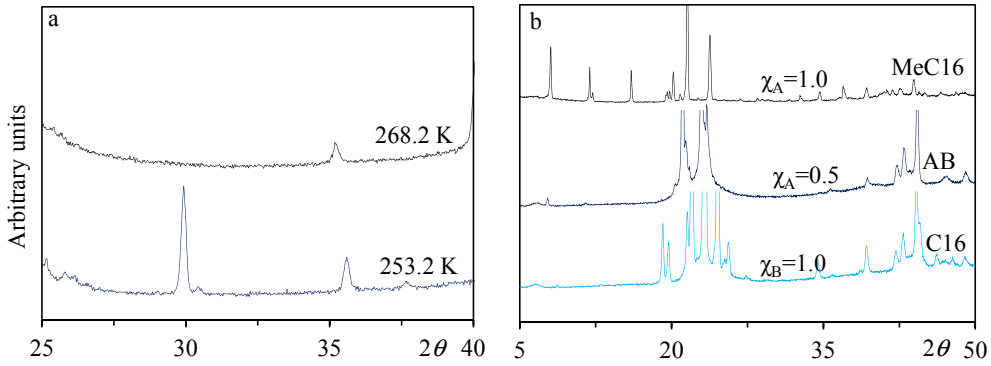

Fig. 14. XRD spectra of the binary system composed by methyl palmitate (A) and hexadecane (B) a) 30% (mol/mol) methyl palmitate; b) At 283 K and the AB co-crystal formed by the 1:1 mixture.

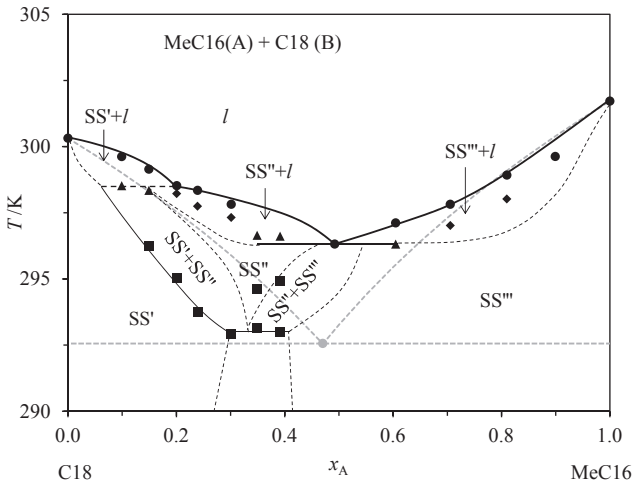

Fig. 15. Solid-liquid phase diagram (p = 0.10 ± 0.01 MPa) for the binary system methyl palmitate (A) + octadecane (B): ● – liquidus line; ■ – solid–solid transition; ▲ – solidus line, ◆ - possible metatectic transition. Dashed grey lines (—) indicates the ideal liquidus line.

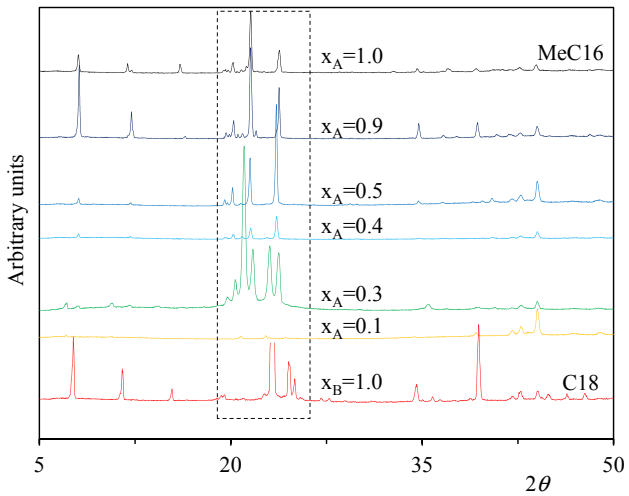

Fig. 17. XRD spectra for the binary system composed by methyl palmitate (A) and octadecane (B) at 295 K.

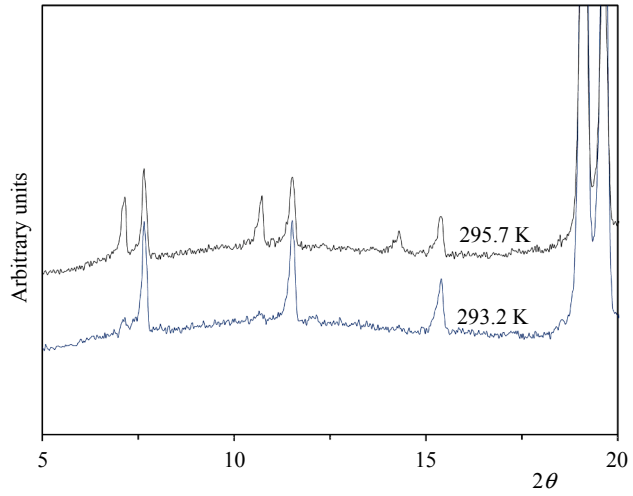

Fig. 16. XRD spectra for the binary system composed by 20% (mol/mol) methyl palmitate and octadecane.

should be present based on the phase rule, optical microscopy and XRD spectra observations. In the region on the left-hand side of the phase diagram, close to the pure eicosane, we found an indication to the formation of a solid-solution. In this region of the phase diagram, there is the formation of a peritectoid at a composition close to x_A = 0.2 and T = 308 K. The initial melting of the mixture of molar fraction x_A = 0.10 at 308 K was detected by optical microscopy and is present as Supporting information (Fig. SI.4).

An eutectoid was also observed at a composition close to x_A = 0.5 and T = 306 K. The melting of the intermediate solid solution SS″ was observed by optical microscopy at x_A = 0.3 and T = 307 K which is presented as supporting information (Fig. SI.4). At the composition range between x_A = 0.1 and x_A = 0.5, an invariant transition at T = 303 K was found. At the same composition region, but at higher temperature, we found the indication for the formation of two biphasic regions, SS′ + SS″ and SS″ + SS‴.

Based on the analysis of the XRD spectra for the different binary compositions, depicted in Fig. 10 we found the indication of a distinct crystal structure pattern for the different compositions supporting the existence of the solid solution. The binary system MeC18 + C20 is characterized by the significant solid phase stabilization as indicated by the rise of the liquidus line temperature when compared with the hypothetical ideal behaviour.

3.4. Phase behaviour of the binary mixture methyl palmitate + eicosane (MeC16 + C20)

The binary system methyl palmitate + eicosane (MeC16 + C20), represented in Fig. 11, presents a solid–liquid phase diagram, similar to the MeC18 + C16 system, with the formation of an eutectic point

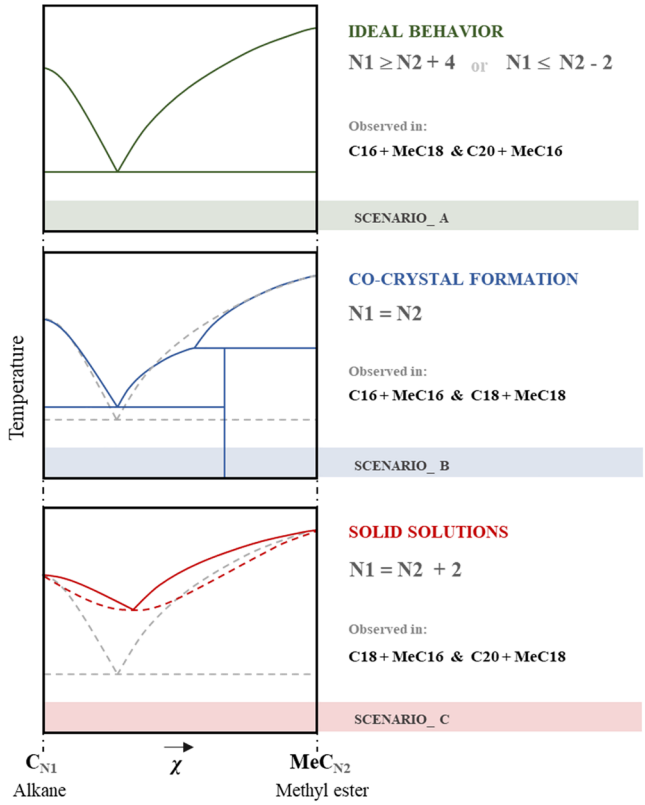

Fig. 18. Schematic diagrams of the phase behaviour of binary mixtures of saturated methyl esters and alkanes and their dependence with the alkyl chain size differences. Dashed line depicts the ideal liquid behaviour described by the Solid-Liquid model.

around 295 K and a composition close to $x_A = 0.8$ as well as a solid–solid transition. The thermograms for this system are depicted in Fig. SI.5. The lower temperature transition is an invariant solid–solid transition at around 280 K which was observed in the compositions region between $x_A = 0.1$ and $x_A = 0.7$. As in previous systems it can be assigned to eicosane crystallizing from solution on a new solid phase not observed in the crystallization from the melt.

3.5. Phase behaviour of the binary mixture methyl palmitate + hexadecane (MeC16 + C16)

The solid–liquid phase diagram for the binary mixture methyl palmitate + hexadecane, (MeC16 + C16) is presented in Fig. 12 and its thermograms are depicted in Fig. SI.6. It shows solid–liquid phase diagram similar than that previously discussed for the system MeC18 + C18.

The liquidus line is in good agreement with the data published by Lobbia et al. [27]. However, our solid–liquid phase diagram results highlights some novel details not previously reported. For molar fractions above $x_A = 0.5$, DSC data suggest the existence of a metatectic transition, as often previously observed in systems with fatty acid esters [20–22], which was further confirmed by optical microscopy. Moreover, the formation of a co-crystal at a 1:1 stoichiometric proportion (AB) was confirmed by the the Tammann plot representation of the solid–solid transition at $T = 259$ K presented in Fig. 13, which indicates the existence of a peritectic point at compositions close to $x_A = 0.4$. This is also supported by the XDR spectra shown in Fig. 14 where the disappearance of the peak at $2\theta = 30^\circ$ at high temperatures is observed.

3.6. Phase behaviour of the binary mixture methyl palmitate + octadecane (MeC16 + C18)

The solid–liquid phase diagram of the system methyl palmitate + octadecane (MeC16 + C18) is presented in Fig. 15 and its thermograms in Fig. SI.7. This binary mixture presents a behaviour similar to the methyl stearate + eicosane (MeC18 + C20) system, with evidences for the formation of a solid-solution in wide ranges of composition. As before the phase diagram presented is based in rationalization of the DSC thermograms, the solid lines corresponding to actual observations of phase transitions while the black dashed lines are the suggestions of the missing phase transitions that should be present based on the phase rule, optical microscopy and XRD spectra observations.

In this binary mixture we observed the formation of a peritectoid in the alkane rich region at a molar fraction of around $x_A = 0.2$ and at 299 K. The eutectoid appears at 293 K at a composition between $x_A = 0.3$–0.4. This transition is supported by the XRD data presented in Fig. 16. At the molar fraction of $x_A = 0.2$ some new diffraction peaks were observed which supports the structural modification expected from the phase diagram proposed.

The eutectic point was found at a molar fraction of about $x_A = 0.5$ and $T = 296$ K. At the methyl palmitate rich region an extensive solid solution region is observed. As for the system methyl stearate + eicosane the existence of the solid solution region is supported by XRD data and optical microscopy as shown in Fig. 17 and Fig. SI.8, respectively.

4. Conclusions

The solid–liquid phase diagrams of the saturated methyl esters and alkanes binary mixtures series show a more complex behaviour than previously reported. Their behaviour follows a pattern that seems to be related with the balance between the size of the methyl ester and the alkane. We found the formation of co-crystals, peritectic and metatectic reactions in mixtures with equal alkyl chain size, and the formation of solid solutions in mixtures of an alkane with a chain two methylene longer than the alkyl chain of the methyl esters. The molecular understanding/interpretation of the phase behaviour of these systems is schematically represented in Fig. 18.

The observed behaviours could be divided in tree typical scenarios organized according the differences in size between the alkyl chains of the mixture components which seem to rule the phase stability. The comparison with the ideal liquid phase model shows a good agreement near the pure compounds and the general conclusions are in good agreement with the results published by Lobbia et al. where a deviation to the ideal eutectic point in the system C16 + MeC16 and an ideal eutectic behaviour as observed for C16 + MeC18 and C16 + MeC19. This last system confirms the conclusion that the ideal eutectic should be forming for the systems represented in Fig. 18, scenario A.

The results here reported and the understanding drawn from the simple binary systems here studied could be extended to the diesel/biodiesel blends phase behaviour interpretation and can be a good model to the interpretation of the increase of the cloud and pour points in biodiesel blends with a rich fraction of methyl palmitate or methyl stearate when combined with mineral diesel with a rich fraction in octadecane or eicosane respectively. The formation of the solid solution in a wide range of concentrations, not previously reported or anticipated, could have important impact on the wax formation as well as in the performance of additives used to improve the low temperatures behaviour of diesel blends.

Declaration of Competing Interest

The authors declare that they have no known competing financial interests or personal relationships that could have appeared to influence the work reported in this paper.

Acknowledgments

This work was developed within the scope of the projects CICECO-Aveiro Institute of Materials, POCI-01-0145-FEDER-007679 (FCT Ref. UID/CTM/50011/2013) and CIQUP, University of Porto (Projects: PEst-UID/QUI/00081/2013): Was also financed by national funds through the Fundação para a Ciência e Tecnologia (FCT/MEC) Portugal, when appropriate co-financed by FEDER under the PT2020 Partnership Agreement and Galp S.A. A.I.M.C.L.F. thanks FCT for the Post-Doc: SFRH/BPD/84891/2012. N.F.M.B. thanks FCT and Galp S.A. for the PhD Research Grant: PD/BDE/113540/2015.

Appendix A. Supplementary data

Supplementary data to this article can be found online at https://doi.org/10.1016/j.fuel.2019.116488.

References

[1] U.S. Energy Information Agency. International Energy Outlook 2013. 2013.
[2] Sarin A. Biodiesel: production and properties. Royal Society of Chemistry; 2012.
[3] Dwivedi G, Jain S, Sharma MP. Impact analysis of biodiesel on engine performance – A review. Renew Sustain Energy Rev 2011;15:4633–41. https://doi.org/10.1016/j.rser.2011.07.089.
[4] Freitas S. Production of biodiesel from the resources endogeneous of timor leste. University of Aveiro; 2013.
[5] Leung DYC, Wu X, Leung MKH. A review on biodiesel production using catalyzed transesterification. Appl Energy 2010;87:1083–95. https://doi.org/10.1016/j.apenergy.2009.10.006.
[6] Boros LAD, Batista MLS, Coutinho JAP, Krähenbühl MA, Meirelles AJA, Costa MC. Binary mixtures of fatty acid ethyl esters: solid-liquid equilibrium. Fluid Phase Equilib 2016;427:1–8. https://doi.org/10.1016/j.fluid.2016.06.039.
[7] Baroutian S, Aroua MK, Raman AAA, Sulaiman NMN. Viscosities and densities of binary and ternary blends of palm oil + palm biodiesel + diesel fuel at different temperatures. J Chem Eng Data 2010;55:504–7. https://doi.org/10.1021/je900299x.
[8] Dwivedi G, Sharma MP. Impact of cold flow properties of biodiesel on engine performance. Renew Sustain Energy Rev 2014;31:650–6. https://doi.org/10.1016/j.rser.2013.12.035.
[9] Knothe G, Krahl J, Van Gerpen J. The Biodiesel Handbook. vol. 1. 2005. doi: 10.1201/9781439822357.
[10] Dunn RO. Effects of minor constituents on cold flow properties and performance of biodiesel. Prog Energy Combust Sci 2009;35:481–9. https://doi.org/10.1016/j.pecs.2009.07.002.
[11] Pérez Á, Casas A, Fernández CM, Ramos MJ, Rodríguez L. Winterization of peanut biodiesel to improve the cold flow properties. Bioresour Technol 2010;101:7375–81. https://doi.org/10.1016/j.biortech.2010.04.063.
[12] Moser BR. Impact of fatty ester composition on low temperature properties of biodiesel-petroleum diesel blends. Fuel 2014;115:500–6. https://doi.org/10.1016/j.fuel.2013.07.075.
[13] Smith PC, Ngothai Y, Dzuy Nguyen Q, O'Neill BK. Improving the low-temperature properties of biodiesel: methods and consequences. Renew Energy 2010;35:1145–51. https://doi.org/10.1016/j.renene.2009.12.007.
[14] Standard AN. ASTM 97-05 Standard Test Method for Pour Point of Petroleum Products. 2005.
[15] Coutinho JAP, Mirante F, Ribeiro JC, Sansot JM, Daridon JL. Cloud and pour points in fuel blends. Fuel 2002;81:963–7. https://doi.org/10.1016/S0016-2361(01)00213-7.
[16] Standardization EC for. EN 116:1997 Diesel and domestic heating fuels – Determination of cold filter plugging point, 1997.
[17] Standardization IO for. ISO 3015:1992 – Petroleum products – Determination of cloud point. 1992.
[18] Knothe G. Dependence of biodiesel fuel properties on the structure of fatty acid alkyl esters. Fuel Process Technol 2005;86:1059–70. https://doi.org/10.1016/j.fuproc.2004.11.002.
[19] Imahara H, Minami E, Saka S. Thermodynamic study on cloud point of biodiesel with its fatty acid composition. Fuel 2006;85:1666–70. https://doi.org/10.1016/j.fuel.2006.03.003.
[20] Maximo GJ, Magalhães AMS, Gonçalves MM, Esperança ES, Costa MC, Meirelles AJA, et al. Improving the cold flow behavior of methyl biodiesel by blending it with ethyl esters. Fuel 2018;226:87–92. https://doi.org/10.1016/j.fuel.2018.03.154.
[21] Costa MC, Boros LAD, Batista MLS, Coutinho JAP, Krähenbühl MA, Meirelles AJA. Phase diagrams of mixtures of ethyl palmitate with fatty acid ethyl esters. Fuel 2012;91:177–81. https://doi.org/10.1016/j.fuel.2011.07.018.
[22] Costa MC, Boros LAD, Coutinho JAP, Krähenbühl MA, Meirelles AJA. Low-temperature behavior of biodiesel: solid-liquid phase diagrams of binary mixtures composed of fatty acid methyl esters. Energy Fuels 2011;25:3244–50.
[23] Benziane M, Khimeche K, Trache D, Dahmani A. Experimental determination and prediction of (solid + liquid) phase equilibria for binary mixtures of aromatic and fatty acids methyl esters. J Therm Anal Calorim 2013;114:1383–9. https://doi.org/10.1007/s10973-013-3147-7.
[24] Benziane M, Khimeche K, Dahmani A, Nezar S, Trache D. Experimental determination and prediction of (Solid + Liquid) phase equilibria for binary mixtures of heavy alkanes and fatty acids methyl esters. J Therm Anal Calorim 2013;112:229–35. https://doi.org/10.1007/s10973-012-2654-2.
[25] Robustillo MD, Meirelles AJA, Pessôa Filho PA. Solid-liquid equilibrium of binary and ternary systems formed by ethyl laurate, ethyl palmitate and dodecylcyclohexane: experimental data and thermodynamic modeling. Fluid Phase Equilib 2016;409:157–70. https://doi.org/10.1016/j.fluid.2015.09.038.
[26] Chabane S, Benziane M, Khimeche K, Trache D, Didaoui S, Yagoubi N. Low-temperature behavior of diesel/biodiesel blends: solid–liquid phase diagrams of binary mixtures composed of fatty acid ethyl esters and alkanes. J Therm Anal Calorim 2018;131:1615–24. https://doi.org/10.1007/s10973-017-6614-8.
[27] Lobbia GG, Berchiesi G, Vitali G. Crystallization curve of hexadecane in mixtures with methyl nonadecanoate, methyl octadecanoate, ethyl octadecanoate, and methyl hexadecanoate. A comparison of the experimental and calculated curves. Thermochim Acta 1983;65:29–33. https://doi.org/10.1016/0040-6031(83)80004-5.
[28] Trache D, Khimeche K, Benelmir R, Dahmani A. DSC measurement and prediction of phase diagrams for binary mixtures of energetic materials' stabilizers. Thermochim Acta 2013;565:8–16. https://doi.org/10.1016/j.tca.2013.04.021.
[29] Trache D, Khimeche K, Benziane M, Dahmani A. Solid-liquid phase equilibria for binary mixtures of propellant's stabilizers. J Therm Anal Calorim 2013;112:215–22. https://doi.org/10.1007/s10973-012-2539-4.
[30] Trache D, Khimeche K, Dahmani A. Study of (Solid-liquid) phase equilibria for mixtures of energetic material stabilizers and prediction for their subsequent performance. Int J Thermophys 2013;34:226–39. https://doi.org/10.1007/s10765-013-1404-4.
[31] Meija J, Coplen TB, Berglund M, Brand WA, De Bièvre P, Gröning M, et al. Atomic weights of the elements 2013 (IUPAC Technical Report). Pure Appl Chem 2016;88:265–91. https://doi.org/10.1515/pac-2015-0305.
[32] Baxter R, Hastings N, Law A, Glass EJ. Perry's Chemical Engineers Handbook. vol. 39. 2008.
[33] Sabbah R, Xu-wu A, Chickos JS, Planas Leitão ML, Roux MV, Torres LA. Reference materials for calorimetry and differential thermal analysis. Thermochim Acta 1999;331:93–204. https://doi.org/10.1002/chin.199936282.
[34] Victoria M, Temprado M, Chickos JS. Critically evaluated thermochemical properties of polycyclic aromatic hydrocarbons. J Phys Chem 2008;37:1855–996. https://doi.org/10.1063/1.2955570.
[35] Costa MC, Sardo M, Rolemberg MP, Coutinho JAP, Meirelles AJA, Ribeiro-Claro P, et al. The solid-liquid phase diagrams of binary mixtures of consecutive, even saturated fatty acids. Chem Phys Lipids 2009;160:85–97. https://doi.org/10.1016/j.chemphyslip.2009.05.004.
[36] Chelouche S, Trache D, Neves CMSS, Pinho SP, Khimeche K, Benziane M. Solid + liquid equilibria and molecular structure studies of binary mixtures for nitrate ester's stabilizers: measurement and modeling. Thermochim Acta 2018;666:197–207. https://doi.org/10.1016/j.tca.2018.07.002.
[37] Chelouche S, Trache D, Pinho SP, Khimeche K, Mezroua A, Benziane M. Solid-Liquid Phase Equilibria, Molecular Interaction and Microstructural Studies on (N-(2-ethanol)-p-nitroaniline + N-(2-acetoxyethyl)-p-nitroaniline) Binary Mixtures. Int J Thermophys 2018;39:129. https://doi.org/10.1007/s10765-018-2452-6.
[38] Costa JCS, Mendes A, Santos LMNBF. Chain length dependence of the thermodynamic properties of n-Alkanes and their monosubstituted derivatives. J Chem Eng Data 2018;63:1–20. https://doi.org/10.1021/acs.jced.7b00837.
[39] Dunn RO. Effects of high-melting methyl esters on crystallization properties of fatty acid methyl ester mixtures. Trans ASABE 2012;55:637–46. https://doi.org/10.13031/2013.41365.
[40] Chickos JS, Zhao H, Nichols G. The vaporization enthalpies and vapor pressures of fatty acid methyl esters C_{18}, $C_{21}$to C_{23}, and C_{25} to C_{29} by correlation – Gas chromatography. Thermochim Acta 2004;424:111–21. https://doi.org/10.1016/j.tca.2004.05.020.
[41] Nikolića R, Marinović-Cincović M, Gadžurić S, Zsigrai IJ. New materials for solar thermal storage — solid/liquid transitions in fatty acid esters. Sol Energy Mat Sol C 2003;79:285–92. https://doi.org/10.1016/S0927-0248(02)00412-9.